Low-Dimensional Materials
https://www.sciltp.com/journals/ldm

Supplementary Materials

Flexible Nanofiber Moisture-Enabled Electric Generator Based on Horizontal Asymmetric Structure

Maoshuang Ran [1], Chunqiao Fu [1], Xulei Lu [1,*], Tingting Yang [1,2]

[1] Tribology Research Institute, School of Mechanical Engineering, Southwest Jiaotong University, Chengdu 610031, China
[2] Institute of Smart City and Intelligent Transportation, Southwest Jiaotong University, Chengdu 611756, China
* Correspondence: lu_xulei@my.swjtu.edu.cn

Table S1. The contrast between horizontal structure and vertical structure.

Ref.		Core Advantage	Mechanical Stability	Encapsulation Difficulty
[1,2], this work	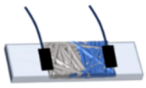 Horizontal structure	Stable structure, easy to integrate	Sturdy, integration, long-life	Low
[3–5]	 Vertical structure	High output power density	Relatively fragile, prone to misalignment	High

Table S2. A comparison of representative MEGs reported in the literature in recent years.

Ref.	Functional Materials	Physical State	Working Principles	Device Geometry	Open Circuit Voltage V_{OC} (V)	Short Circuit Current Density J_{SC} (μA/cm²)	Power Density $P_M = V_{OC} \times J_{SC}$ (nW/cm²)	Operating Humidity (%)
[3]	Cellulose Acetate	Electrospun nanofiber membrane	Directed ion migration	Vertical structure	0.3	0.08	8	85
[4]	Lignin sulfonate-Al^{3+}-PAA hydrogel	Hydrogel	Directed ion migration + Redox	Vertical structure	0.55	3.28	-	55
[5]	SF/PEO/Sericin	Electrospun nanofiber membrane	Directed ion migration	Vertical structure	0.18	0.0175	1.3	95
[6]	(PSSA-PVA)/(HPC-KGM)	Aerogel	Directed ion migration	Vertical structure	1.1	0.0089	9.79	20
[7]	PSSA-PDDA	Polymer composite film	Directed ion migration	Vertical structure	0.95	0.05	47.5	25
[8]	SAlignin	Electrospun nanofiber membrane	Directed ion migration	Vertical structure	0.28	0.125	44.5 W/kg	99
[9]	PEO	Electrospun nanofiber membrane	Directed ion migration	Vertical structure	0.83	30	24.3	99
[10]	TiO_2/ZrO_2	Electrospun nanofiber membrane	Directed ion migration	Vertical structure	~0.8	~0.001	-	99
[2]	SO_4-MOF-808/ZIF-8	Modified filter paper	Directed ion migration	Horizontal structure	0.2	20.6	270	65
This work	Al/SDBS	Electrospun nanofiber membrane	Directed ion migration + Redox	Horizontal structure	0.06	0.375	43.3	93

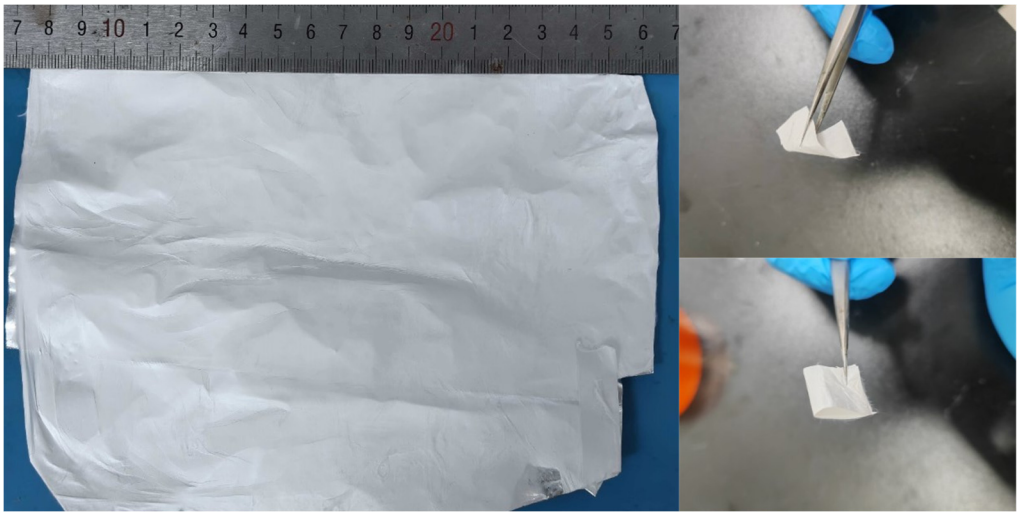

Figure S1. PAN nanofiber film. The film is flexible and can be bent and folded at will.

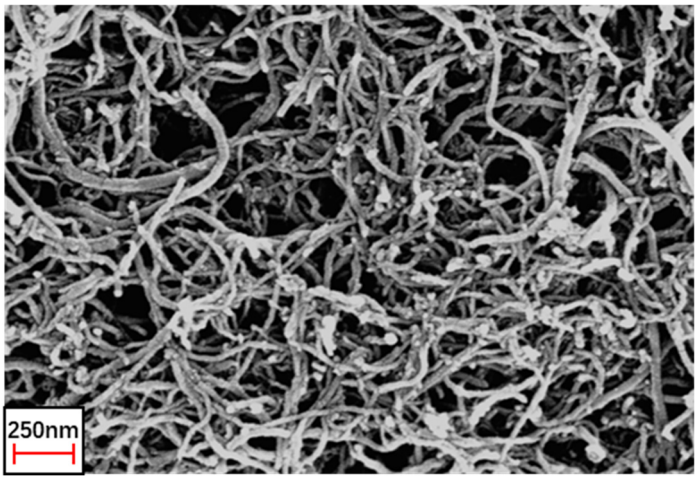

Figure S2. SEM image of CNT distribution on the surface of PAN nanofiber films.

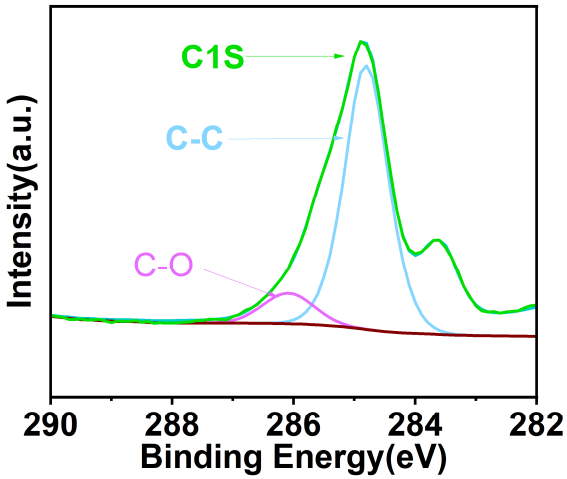

Figure S3. XPS diagram of PAN nanofiber film impregnated with CNT. The main peak at approximately 284.6–284.8 eV is the strongest peak, corresponding to C-C, mainly derived from the PAN molecular skeleton and the graphitized carbon structure of CNT, which is the main component of the carbon material in the composite film. A secondary peak can be observed near 286.0 eV, which usually belongs to C-O and is related to the hydroxyl (-OH) or ether bonds introduced on the CNT surface, indicating that a certain degree of oxidative functionalization has occurred on the CNT surface [11].

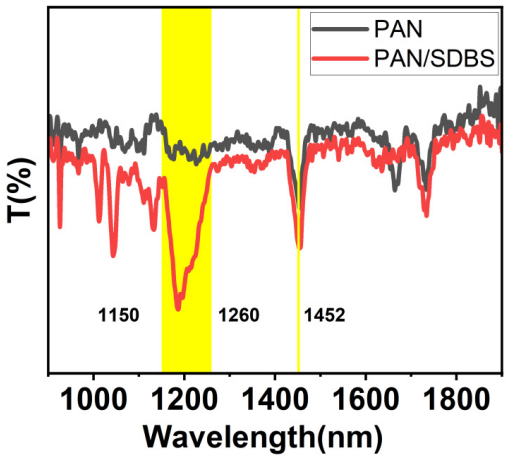

Figure S4. FTIR results of the original PAN nanofiber film and the PAN nanofiber film with SDBS. The weak absorption peak in the 1260–1150 cm^2 region and the new absorption band in the 1452 cm^2 region can be attributed to the vibration of the C-O-C bond combination and the symmetrical bending of $-CH_2$, which is related to the addition of SDBS, indicating its successful incorporation into nanofibers [12].

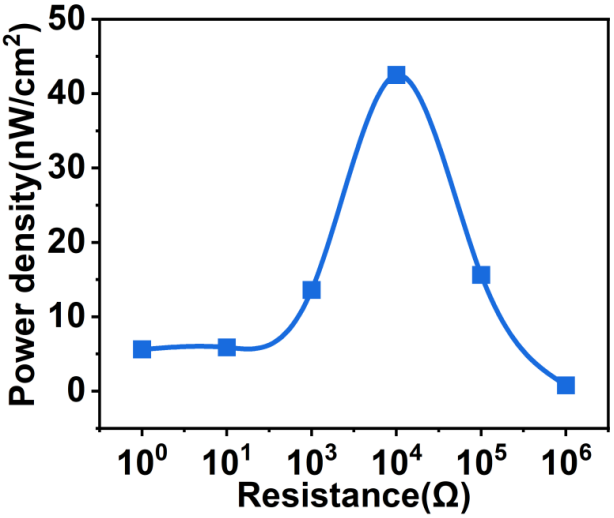

Figure S5. Power density with variable external resistance.

Figure S6. On-site testing equipment.

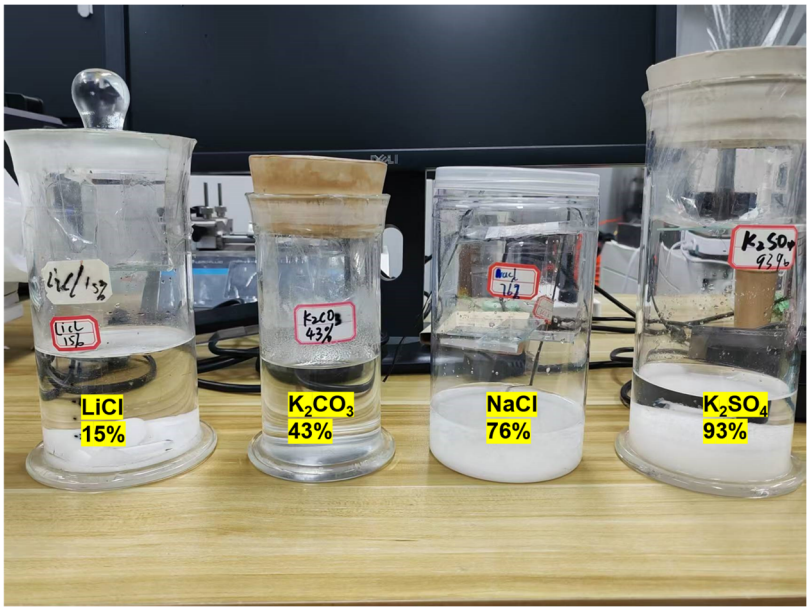

Figure S7. Humidity test environment.

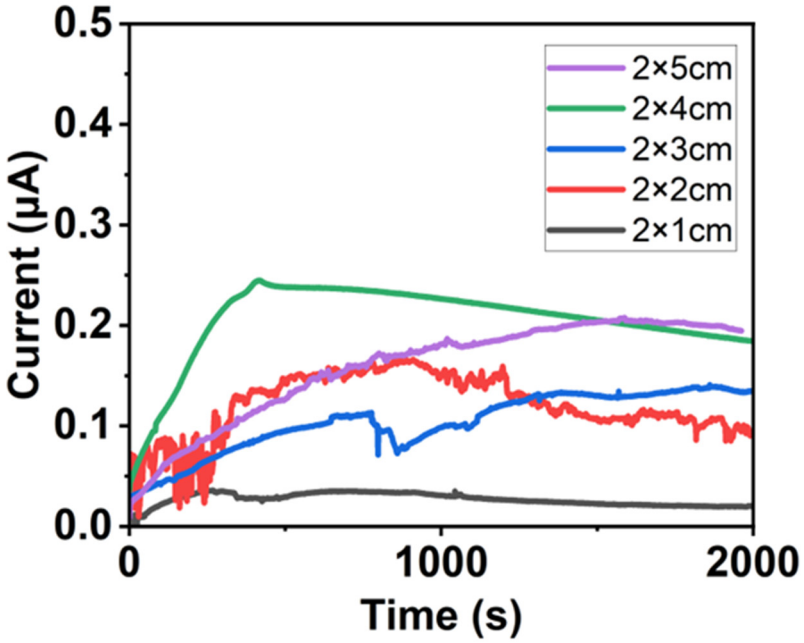

Figure S8. Short-circuit current output of HAMEG under different film lengths. The HAMEG was soaked three times with SDBS and CNT, respectively. The experiment was conducted at room temperature and 93%RH. When the film length was less than 4 cm, the performance of HAMEG was poor. This could be due to the insufficient film length, which limits the amount of SDBS introduced and reduces the ion concentration gradient, resulting in lower performance. On the other hand, when the film length exceeded 4 cm, the performance of HAMEG also decreased, likely because the ion transport distance became too long, leading to an insufficient driving force from the ion concentration gradient and fewer ions reaching the opposite end.

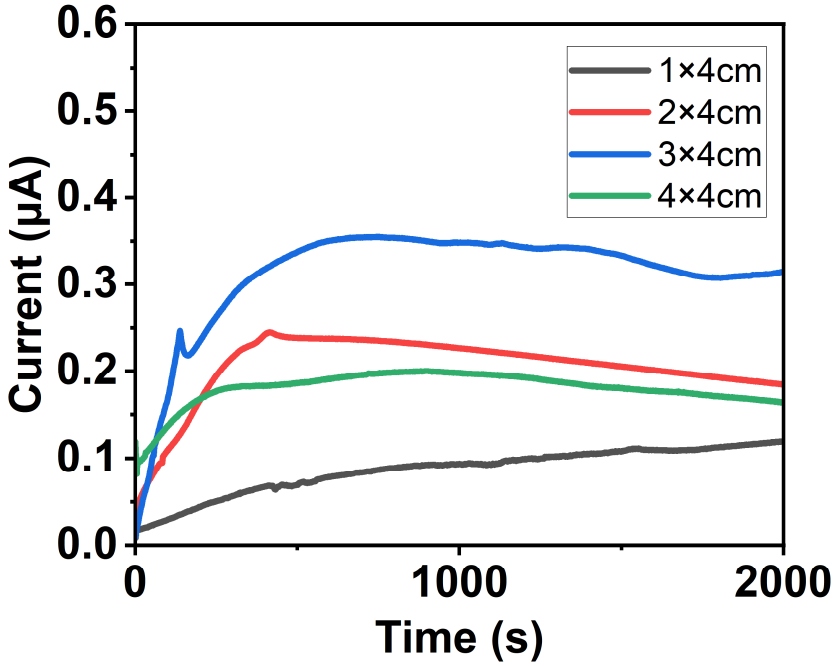

Figure S9. Short-circuit current output of HAMEG under different film width. The HAMEG was soaked three times with SDBS and CNT, respectively. The experiment was conducted at room temperature and 93%RH. When the width of the film is less than 4cm, the performance of HAMEG improves with the increase in width. This might be because the increase in the amount of SDBS enables the dissociation of more ions. However, when the width reaches 4 cm, the performance of HAMEG does not improve, which might be due to certain obstacles in the horizontal transport of ions.

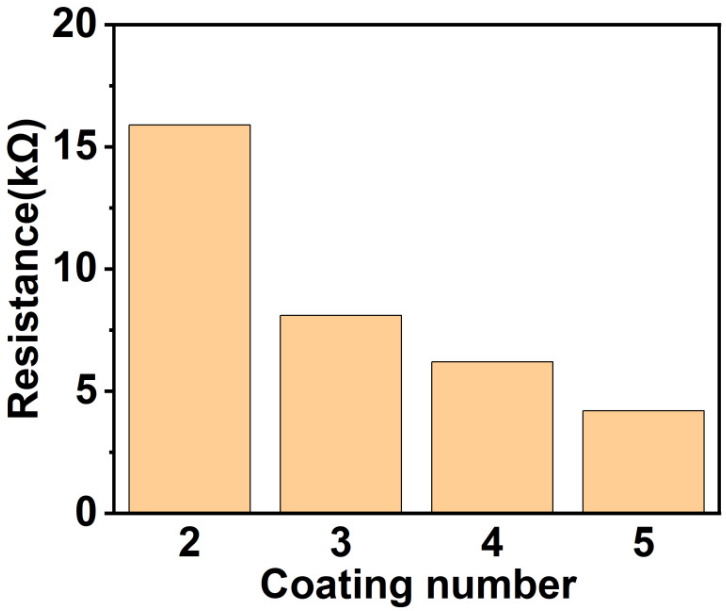

Figure S10. Thin-film resistors under different CNT impregnation times. As the number of impregnations increases, the resistance gradually decreases.

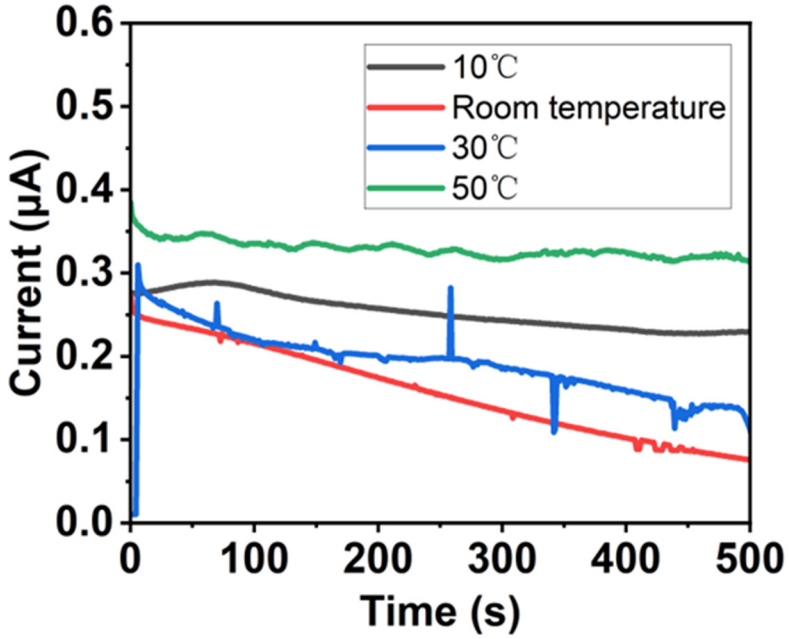

Figure S11. Short-circuit current output of HAMEG under different temperature. The HAMEG was soaked three times with SDBS and CNT, respectively. The experiment was conducted at room temperature and 93% RH. Overall, the short-circuit current increases with the rise in temperature, which can be attributed to the enhanced ion mobility and the accelerated kinetics of moisture adsorption. It is worth noting that a relatively high current output was also observed at 10 °C, which might be due to the improved moisture retention of the hygroscopic components, compensating for the reduction in ion mobility. These results indicate that the device can operate over a wide temperature range, although research on the temperature dependence of the system will be conducted in future work.

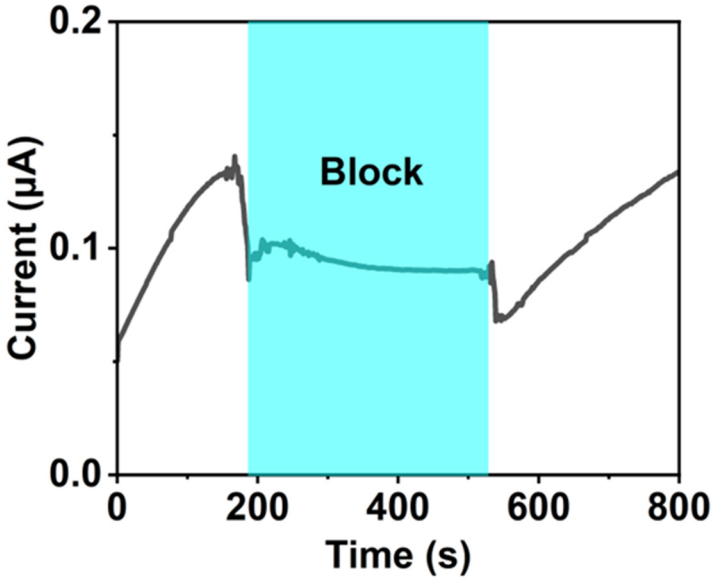

Figure S12. The short-circuit current signal changes before and after being covered at the impregnated SDBS of the device.

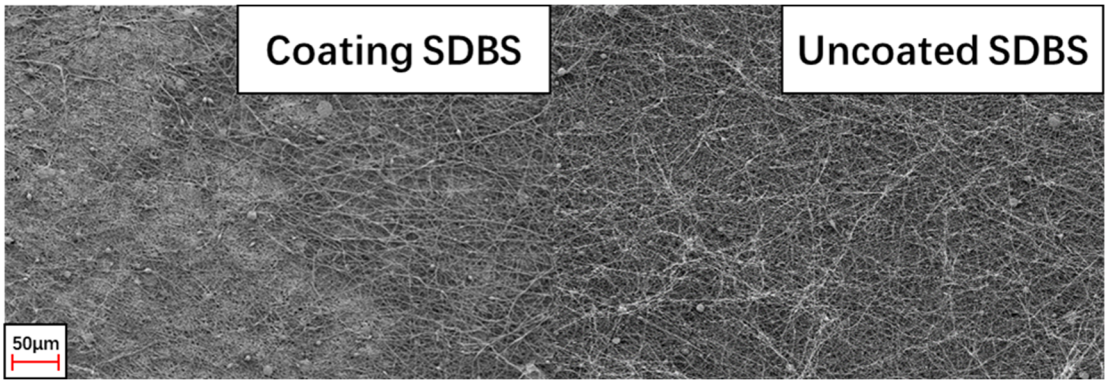

Figure S13. SEM image at the EDS scanning point.

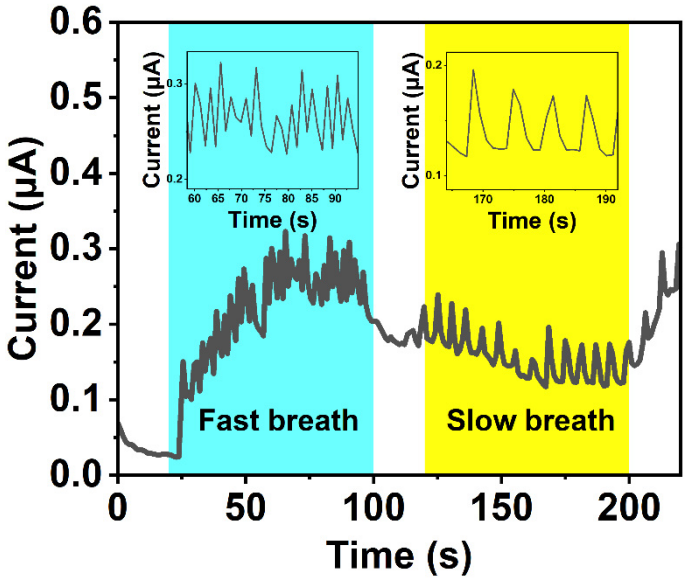

Figure S14. Short-circuit current output of HAMEG at different respiratory rates. At different breathing rates, the short-circuit current signal output by HAMEG varies, among which rapid breathing generates a higher and faster current response.

References

1. Zhang, Y.; Guo, S.; Yu, Z.G.; et al. An Asymmetric Hygroscopic Structure for Moisture-Driven Hygro-Ionic Electricity Generation and Storage. *Adv. Mater.* **2022**, *34*, 2201228.
2. Fauziah, A.R.; Schöfbeck, F.; Reithofer, M.R.; et al. Self-Powered Flexible Janus-like Metal-Organic Framework Membrane for Sustainable Moisture-Enabled Electrokinetic Energy Harvesting. *J. Mater. Chem. A* **2026**. https://doi.org/10.1039/D5TA06289F.
3. Lyu, Q.; Peng, B.; Xie, Z.; et al. Moist-Induced Electricity Generation by Electrospun Cellulose Acetate Membranes with Optimized Porous Structures. *ACS Appl. Mater. Interfaces* **2020**, *12*, 57373–57381.
4. Zhang, J.; Zhuang, J.; Lei, L.; et al. Rapid Preparation of a Self-Adhesive PAA Ionic Hydrogel Using Lignin Sulfonate–Al^{3+} Composite Systems for Flexible Moisture-Electric Generators. *J. Mater. Chem. A* **2023**, *11*, 3546–3555.
5. He, H.; Zhang, J.; Pan, J.; et al. Moisture-Enabled Electric Generators Based on Electrospinning Silk Fibroin/Poly (Ethylene Oxide) Film Impregnated with Gradient-Structured Sericin. *ACS Appl. Energy Mater.* **2024**, *7*, 2980–2988.
6. Zhao, K.; Li, S.; Zan, G.; et al. Moisture-Driven Energy Generation by Vertically Structured Polymer Aerogel on Water-Collecting Gel. *Nano Energy* **2024**, *126*, 109645.
7. Wang, H.; Sun, Y.; He, T.; et al. Bilayer of Polyelectrolyte Films for Spontaneous Power Generation in Air up to an Integrated 1,000 V Output. *Nat. Nanotechnol.* **2021**, *16*, 811–819.
8. Zheng, H.; Zhou, A.; Li, Y.; et al. A Sandwich-like Flexible Nanofiber Device Boosts Moisture Induced Electricity Generation for Power Supply and Multiple Sensing Applications. *Nano Energy* **2023**, *113*, 108529.
9. Sun, Z.; Feng, L.; Xiong, C.; et al. Electrospun Nanofiber Fabric: An Efficient, Breathable and Wearable Moist-Electric Generator. *J. Mater. Chem. A* **2021**, *9*, 7085–7093.
10. Wang, L.; Feng, L.; Sun, Z.; et al. Flexible, Self-cleaning, and High-Performance Ceramic Nanofiber-Based Moist-

Electric Generator Enabled by Interfacial Engineering. *Sci. China Technol. Sci*. **2022**, *65*, 450–457.

11. Akhtar, M.S.; Li, Z.Y.; Park, D.M.; et al. A New Carbon Nanotubes (CNTs)–Poly Acrylonitrile (PAN) Composite Electrolyte for Solid State Dye Sensitized Solar Cells. *Electrochim. Acta* **2011**, *56*, 9973–9979.
12. Sun, Z.; Wen, X.; Wang, L.; et al. Capacitor-Inspired High-Performance and Durable Moist-Electric Generator. *Energy Environ. Sci*. **2022**, *15*, 4584–4591.